NASA Technical Memorandum 104514

On Protection of Freedom's Solar Dynamic Radiator from the Orbital Debris Environment Part 2: Further Testing and Analyses

Jennifer L. Rhatigan
Lewis Research Center
Cleveland, Ohio

Eric L. Christiansen
Lyndon B. Johnson Space Center
Houston, Texas
and

Michael L. Fleming
LTV Missiles and Electronics
Dallas, Texas

Prepared for the
International Solar Energy Conference
sponsored by the American Society of Mechanical Engineers
Lahaina, Maui, Hawaii, April 4-8, 1992

NASA

ON PROTECTION OF FREEDOM'S SOLAR DYNAMIC RADIATOR FROM THE ORBITAL DEBRIS ENVIRONMENT

PART 2: FURTHER TESTING AND ANALYSES

Jennifer L. Rhatigan
National Aeronautics and Space Administration
Lewis Research Center
Cleveland, Ohio 44135

Eric L. Christiansen
National Aeronautics and Space Administration
Lyndon B. Johnson Space Center
Houston, Texas 77058

and

Michael L. Fleming
LTV Missiles and Electronics Corporation
Dallas, Texas 75265

ABSTRACT

Recent progress to better understand the environmental threat of micrometeoroid and space debris to the radiator for the solar dynamic power system on Space Station Freedom is reported. The objective has been to define a design which would perform to survivability requirements over the expected lifetime of the radiator.

A previous paper described the approach developed to assess on-orbit survivability of the solar dynamic radiator due to micrometeoroid and space debris impacts. Preliminary analyses were presented to quantify the solar dynamic radiator survivability. These included the type of particle and particle population expected to defeat the radiator bumpering. Results of preliminary hypervelocity impact (HVI) testing performed on radiator panel samples were also presented.

This paper presents results of a more extensive test program undertaken to further define the response of the solar dynamic radiator to HVI. Tests were conducted on representative radiator panels (under ambient, nonoperating conditions) over a range of particle size, particle density, impact angle, and impact velocity. Target parameters were also varied. Data indicate that analytical penetration predictions are conservative (i.e., pessimistic) for the specific configuration of the solar dynamic radiator.

Test results are used to define the solar dynamic radiator reliability with respect to HVI more rigorously. Test data, analyses, and survivability results are presented.

NOMENCLATURE

c_{ms} coefficient in multishock equation (cm^3-s/km-g)

c_n coefficient in nonoptimum Whipple shield equation [km-$g^{2/3}$/(s-$cm^{5/2}$)]

c_p coefficient in radiator extrusion perforation correlation $[\text{km-g/(cm-s)}]^{1/3}$

d projectile diameter (cm)

d_c critical projectile diameter causing failure (cm)

S spacing from front wall (bumper) to backwall (extrusion) (cm)

ΣS_i total spacing between first bumper and back wall (cm); that is, sum of all interplate spacings in multishock shield configuration.

t_2 back wall or extrusion wall thickness (cm)

V impact velocity (km/sec)

V_n normal impact velocity (km/sec), $V_n = V \cos\Theta$

ρ_p projectile density (g/cm^3)

ρ_1 facesheet (bumper) density (g/cm^3)

σ_{y2} back wall yield stress (ksi)

Θ impact obliquity angle measured from surface normal (deg)

BACKGROUND

The solar dynamic radiator (SDR) is designed to perform as the thermal sink for the Closed Brayton Cycle solar dynamic power system on Space Station Freedom. The solar dynamic power system and the SDR have been described in detail elsewhere.(14,10) A previous paper (13) gave an overview of the preliminary testing and analyses performed to initially quantify the probable survivability of the SDR over its lifetime in the orbital debris environment.

This paper describes further testing and analysis undertaken to achieve a better understanding of the response of the SDR to the environmental threat of hypervelocity impact (HVI) from micrometeoroids and space debris. This component of space hardware is unique enough in configuration such that previously developed survivability prediction techniques cannot provide adequate insight as to whether the radiator design could meet the required probability of survival over the 10 year lifetime in low-earth orbit. In addition, no satisfactory technique existed to evaluate design changes

made to improve radiator protection from orbital debris impacts. Thus a program of testing and analysis was initiated to ensure that the survivability requirements could be met.

This particular study focuses upon design of the radiator *panels* for survivability under hypervelocity impacts. Survivability of other radiator components was discussed in the previous paper. Figure 1 illustrates the configuration of the radiator panels, designed to efficiently reject waste heat from the flow tubes (coolant passages), through the extruded bumpering around the tubes, and

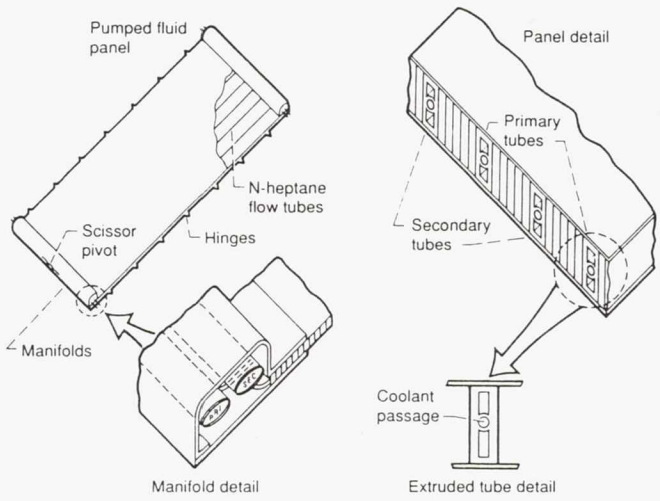

Figure 1.—Solar dynamic module radiator panel.

finally to the outer surface, which is coated with a highly emissive white paint. Paramount to successful radiator operation is maintenance of a sealed, and unobstructed, coolant flow path. An environmental threat to the radiator panels is that hypervelocity impact from a micrometeoroid or debris particle could puncture a flow tube. For this reason, among others, the radiator is designed with an entirely redundant flow path to be used if the primary flow path cannot function.

The previous paper (13) reported results of a series of 12 HVI tests performed on SDR panel samples. That test series has been designated 'phase 1' of the current program. The results presented herein are referred to as 'phase 2' results.

OBJECTIVES FOR SECOND PHASE OF TESTING

The objective of this study was to refine the phase 1 meteoroid and debris penetration assessment for the SDR. The phase 2 test methodology was designed to establish the effect of impact angle (obliquity) and to characterize the "impact limit" of the flow tubes within the panels; that is, the impact conditions that just cause failure (penetration) of the flow tubes. (Failure is defined as flow tube penetration. "Pinching" of a tube is not considered a failure as the radiator can continue to operate under this condition because of the parallel flow configuration.) In addition, protection benefits associated with an increase in tube wall thickness were determined. Some limited testing to assess projectile velocity effects and effects of HVI on the panel coating were also performed.

SECOND PHASE OF HYPERVELOCITY IMPACT TESTING

Test Facility

As with the first test phase, the NASA Johnson Space Center (JSC) Hypervelocity Impact Research Laboratory (HIRL) performed the second phase of SDR HVI testing. This study used the HIRL 4.3 mm gun (launch tube bore diameter) which is capable of launching 3.2 mm diameter spherical projectiles at 7 km/sec. Diagnostic data on the tests were obtained by using a high-speed laser-shadowgraph framing camera. The camera is used to confirm projectile velocity and integrity, and to provide impact data such as ejected particle pattern and velocity.(5,12)

Test Articles. Four types of test articles were used for evaluation in the second phase of HVI testing. These are shown in Figure 2(a). The test articles contain extruded aluminum flow tubes sandwiched between aluminum honeycomb. This matrix is bonded between 0.010 in. aluminum facesheets (Fig. 3). Samples 1

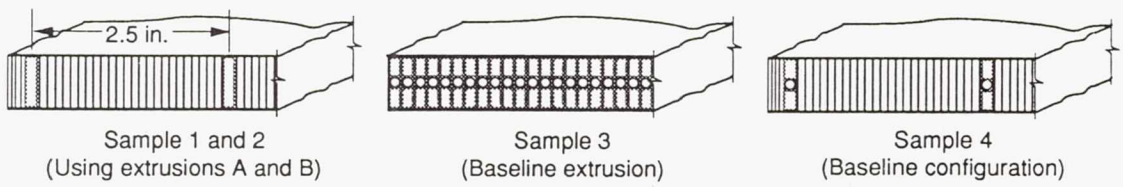

Figure 2A.—Details of Hypervelocity test sample to maximize useful test results.

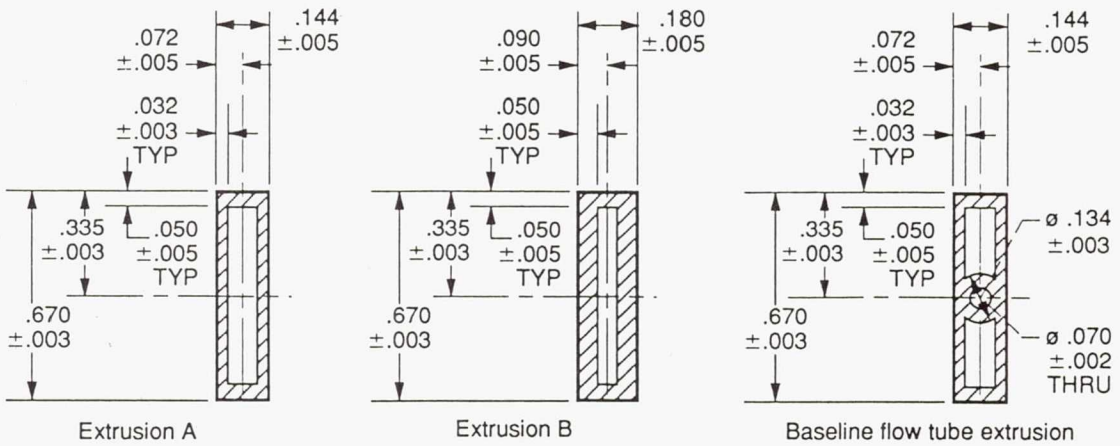

Figure 2B.—Test sample extrusion details.

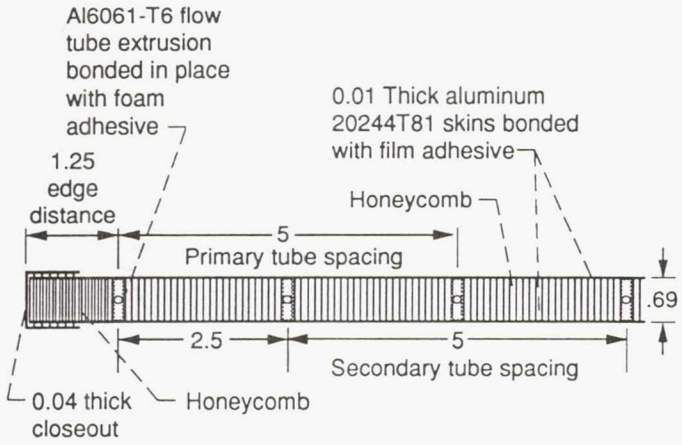

Figure 3.—Details of SDR panel design (All dimensions in inches; 1 inch = 2.54 CM).

and 2 differ only in the extrusion wall thickness (0.032 in. versus 0.05 in., Fig. 2(b)). As discussed in the phase 1 report, (13) the configurations of sample types 1 to 3 were selected to increase the data return from HVI testing by increasing the target size while maintaining realistic HVI response characteristics. Type 4 samples -- the baseline SDR configuration -- were used to verify experimental findings by repeating test conditions. A single side of some of the type 4 test panels is coated with Z-93 zinc-oxide white paint (nominally 0.06 in. thick layer); a candidate radiator thermal coating. This allowed impact evaluation of a potential radiator thermal coating, albeit under ambient, nonoperating thermal conditions.

Test Procedure. Test conditions for 33 hypervelocity impact tests conducted during the second phase of the SDR testing are given in Table I. The majority of the tests were conducted with round aluminum projectiles to simulate the density (but not necessarily the shape) of orbital debris. Because meteoroids have a lower density (0.5 g/cm^3), two tests were performed with nylon spherical projectiles to assess projectile density effects. Projectile sizes from 1.0 mm to 2.4 mm were used, with obliquity angles varying up to 75° from the surface normal. All but two tests were performed with the shot line direction perpendicular (normal) to the axis of the flow tube; the shot direction of the two exceptions was parallel to the flow tube.

Figure 4 illustrates the test setup. An aluminum "witness plate" (typically 0.4 mm A16061-0) was placed 2.5 cm behind the

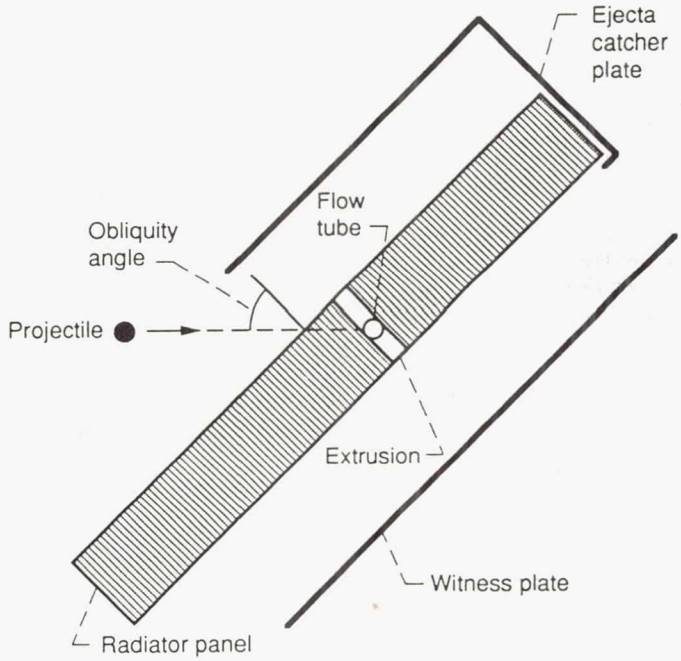

Figure 4.—Test setup.

TABLE I. - IMPACT CONDITIONS

HIRL Shot Number	Projectile Diameter (mm)	Velocity (km/s)	Impact Angle (degrees)	Projectile Density (g/cc)	Mass (mg)	Target Type *	Spacing (mm)	Direction
A1033	1.42	7.8	45	2.8	4.2	Sample 1	12.3	Normal
A1034	1.59	6.0	45		5.9		5.2	
A1048	1.00	6.5	45		1.5		8.7	
A1049	1.59	6.4	45		5.9	↓	18.6	
A1050	2.38	6.2	45		19.7	Sample 2	0.0	
A1051	1.59	6.9	45		5.9		0.0	
A1052	2.38	6.1	45		19.7	↓	11.6	
A1054	1.59	6.6	45		5.9	Sample 1	13.7	
A1056	1.59	6.8	45		5.9	Sample 2	5.7	
A1057	1.59	6.4	60		5.9		8.3	
A1070	2.38	7.0	60		19.7	↓	8.3	
A1071	2.00	6.5	60		11.7	Sample 1	24.4	
A1072	2.00	6.6	60		11.7		0.0	
A1073	2.00	5.9	60		11.7		27.9	
A1075	2.00	6.5	60		11.7	↓	4.2	
A1089	2.00	6.5	60		11.7	Sample 2	10.6	
A1092	1.59	6.7	0		5.9	Sample 3	0.0	↓
A1093	1.59	6.9	45		5.9	Sample 3	0.0	Parallel
A1094	2.00	6.8	45		11.7	Sample 4-B	22.2	Normal
A1095	2.00	5.2	45		11.7	Sample 4-F	9.4	
A1096	2.38	6.6	75		19.7	Sample 2	37.0	
A1097	2.38	6.8	75	↓	19.7	Sample 1	23.5	
A1098	2.38	6.5	45	1.1	8.0	Sample 1	10.1	
A1099	1.80	6.8	0	2.8	8.5	Sample 3	0.0	↓
A1101	1.80	6.6	45		8.5	Sample 3	0.0	Parallel
A1104	2.00	6.6	45		11.7	Sample 2	5.3	Normal
A1105	2.00	3.4	45		11.7	Sample 1	23.6	
A1106	2.00	7.2	45		11.7		24.7	
A1108	2.00	7.0	45		11.7	↓	19.3	
A1109	2.00	6.7	45	↓	11.7	Sample 2	8.1	
A1185	2.38	5.7	45	1.1	8.0	Sample 4-F	12.6	
A1186	2.00	6.1	45	2.8	11.7		1.5	
A1188	2.00	3.7	45	2.8	11.7	↓	13.2	↓

*Target Type Note : B indicates coating on back and F indicates coating on front (for Sample 4)

test panel to gauge the effects from products of penetration. The "ejecta catcher" in front of the panel was used to record the damaging effects of particles ejected from the front surface of the panel. Typically, the ejecta catcher was 0.3 mm A1 6061-0, but A1 3003-H12 ejecta catchers up to 0.64 mm thick were used for some shots, such as the very high obliquity shots, which generated particularly damaging ejecta.

Test velocities ranged up to 7.8 km/sec. It is estimated that only about 25 percent of all orbital debris impacts will occur at 8 km/sec or less, but this is currently the highest velocity available experimentally in the particle range of interest. The average impact velocity for orbital debris at Space Station Freedom altitude is over 10 km/sec, while average meteoroid velocity is 20 km/sec. Thus some method is needed to scale the experimental results to velocities experienced on-orbit. The approach of this study is to use the lower speed test data to modify existing semi-empirical models that have been previously developed for dual multiplate aluminum structures.(1-4) Semi-empirical predictor equations combine HVI test data with an analytical or theoretical basis for scaling to higher velocities. But given the complex geometry of the radiator panels, with internal honeycomb, thick bonding adhesive layer, and nonparallel surfaces, some adjustment of the semi-empirical equation parameters become necessary. These modifications are based on the test data.

Low speed impacts can sometimes be more damaging to spaced shields because less projectile fragmentation occurs.(1) Consequently, a few tests were conducted to determine if damage to the radiator structure at lower velocities is more or less severe.

RESULTS FROM SECOND PHASE OF HVI TESTING

HVI Data

Data on the extent of damage to the radiator panels from the second phase of HVI testing is listed in Table II. Comments on the damage to the bumper interior section and flow tube (if applicable) of the extrusion are given. A simple leak check was performed to determine if an extrusion was perforated (completely penetrated) by filling the extrusion with water under ambient conditions (unpressurized) and checking for leaks. Perforation is considered failure. Damage to nonperforated extrusions is indicated by the extent of closure or "pinching" of the flow tube.

In addition to perforation assessment, general damage to the facesheet and honeycomb was assessed. Facesheet hole sizes were measured from the inside of the hole. The front facesheet holes were generally elliptical with the long axis parallel to the direction of projectile flight, but became more irregular as obliquity angles increased. The Z93 white paint partially spalled (that is, it was ejected by the impact shock) from a small area around the front facesheet impact hole. The coating spall size was typically 4 to 6 times the diameter of the projectile at the impact conditions tested. Back facesheet damage given in Table II only indicates the hole measured at the surface of the panel. Much more extensive damage occurs to the back facesheet from tearing and petaling of the facesheet. The honeycomb damage size is a rough measure of the area of crushed and ejected honeycomb.

Figure 5 shows the result of a 2.38 mm aluminum sphere impacting at a 60° angle at 6.95 km/sec (HIRL Shot A1070). Note the small entrance hole on the front sheet and the petalled hole in the back facesheet. Generally, high obliquity shots had less rear facesheet petaling; that is, a 45° shot exhibited a larger petalled area than an equivalent 60° shot. However, the witness plates mounted behind oblique shots do not have a great deal of damage. As displayed in Fig. 5, the witness plate is coated with black powder debris and is severely deformed, but only exhibits a few fragment impacts that left dimples on the witness back surface and no perforations. This indicates that the projectile debris that exited the panel contained no large fragments and produced a primarily impulsive load to the witness plate.

The ejecta catcher plates, on the other hand, had multiple perforations with many of these concentrated near the surface of the panel. As demonstrated by comparing the damage patterns in the ejecta catchers, the damage from secondary ejecta debris increases substantially as impact obliquity angle increases. A detailed analysis of the ejecta catchers should be performed to correlate damage extent with impact conditions, and to make quantitative predictions of the secondary debris hazards to nearby structures such as the solar dynamic concentrator assembly.

Damage to a coated radiator panel from HVI is given in Fig. 6. A 2.0 mm aluminum sphere impacting at 45° and 6.83 km/sec created a petalled hole on the coated facesheet of the rear of the panel. The coating remained relatively intact, and even adhered to a large portion of the surface area of the petals in the facesheet.

TABLE II. - TEST ARTICLE DAMAGE MEASUREMENTS

HIRL Shot Number	Bumper Interior Damage *	Flow Tube Damage *	Front Facesheet Hole Size Max (mm)	Front Facesheet Hole Size Min (mm)	Back Facesheet Hole Size Max (mm)	Back Facesheet Hole Size Min (mm)	Honeycomb Hole Size Max (mm)	Honeycomb Hole Size Min (mm)	Coating Spall Size (mm x mm)
A1033	None	N/A	3.6	3.1	1.4	0.2	21.0	18.0	N/A
A1034	Bulge (100%)		4.5	3.4	0.1	0.1	35.5	22.0	
A1048	None		2.9	2.5	3.5	3.4	9.0	6.0	
A1049	None		4.5	3.5	6.5	3.7	18.5	15.5	
A1050	Perforated		19.0	13.0	0.0	0.0	Not Measured	Not Measured	
A1051	Perforated		12.5	11.0	0.0	0.0	Not Measured	Not Measured	
A1052	Perforated		6.6	4.5	4.5	4.0	55.5	33.0	
A1054	Bulge (30%)		4.3	3.4	4.2	4.2	29.5	17.5	
A1056	Bulge (10%)		6.5	4.5	45.5	22.5	Not Measured	Not Measured	
A1057	Slight Bulge (<10%)		4.8	3.4	0.0	0.0	22.5	13.0	
A1070	Perforated		8.0	5.0	9.0	7.5	42.0	32.5	
A1071	None		6.3	4.0	7.0	4.5	22.5	20.0	
A1072	Perforated		2.7	2.7	0.0	0.0	Not Measured	Not Measured	
A1073	None		6.2	4.3	8.5	3.5	23.0	16.5	
A1075	Perforated		7.5	4.0	8.5	4.0	35.5	22.0	
A1089	Bulge (90%)	↓	6.2	3.9	7.5	4.0	38.0	35.5	
A1092	Perforated	Perforated	4.8	4.8 *	0.0	0.0	N/A	N/A	
A1093	Perforated	None	5.2	5.2	0.0	0.0	N/A	N/A	↓
A1094	Bulge (10%)	None	5.3	4.3	3.0	3.0	22.5	17.0	None
A1095	Perforated	None	5.5	4.0	6.0	4.5	24.5	13.0	11.5 x 9.0
A1096	None	N/A	10.5	4.0	2.5	2.0	26.0	18.5	N/A
A1097	None		9.5	4.0	5.0	3.5	21.5	16.0	
A1098	Bulge (30%)	↓	5.2	4.3	10.5	3.5	37.0	20.0	
A1099	Perforated	Perforated	7.0	6.5	0.0	0.0	N/A	N/A	
A1101	Perforated	Pinched (100%)	6.5	6.0	0.0	0.0	N/A	N/A	
A1104	Perforated	N/A	8.0	6.5	8.0	7.5	43.0	31.0	
A1105	None		4.6	3.1	8.5	4.5	16.5	7.0	
A1106	None		6.0	5.0	21.5	6.5	Not Measured	Not Measured	
A1108	Bulge (20%)		5.0	3.5	7.5	3.5	35.5	19.0	
A1109	Perforated	↓	5.5	3.5	6.0	6.0	43.5	28.5	↓
A1185	None	None	5.3	4.3	10.2	10.2	Not Measured	Not Measured	11.4 x 10.2
A1186	Perforated	None	6.6	5.1	10.7	7.6	Not Measured	Not Measured	16.5 x 12.7
A1188	Bulge (30%)	None	4.6	3.3	7.6	7.6	Not Measured	Not Measured	10.7 x 9.7

*Bumper Interior damage Note: Bulge (x%) = x% of tube closed (estimated)
*Flow Tube Damage Note: Pinched (x%) closed (estimated)

HIRL shot A1070
Projectile 2.380 mm Al-2017T4
Velocity 6.95 km/sec
Impact angle 60 degrees

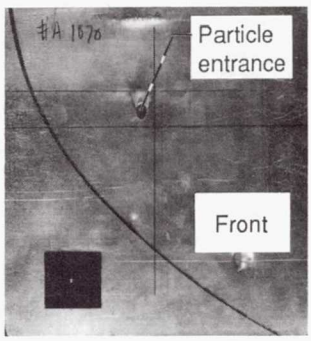

(a) Front of test article.

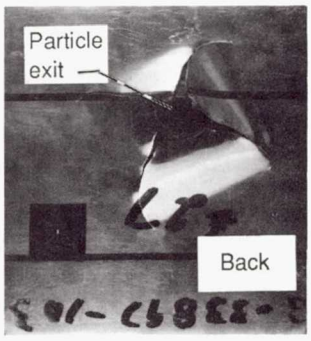

(b) Back of test article.

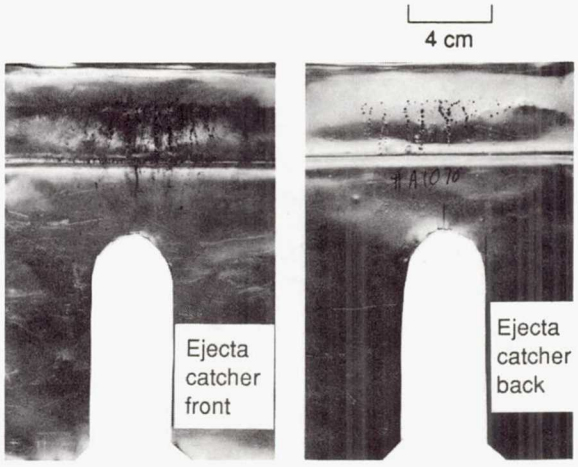

Ejecta catchers, (c) front; (d) back; "unfolded" from test configuration.

Figure 5.—Example of test article damage.

HIRL shot A1070
Projectile 2.380 mm Al-2017T4
Velocity 6.95 km/sec
Impact angle 60 degrees

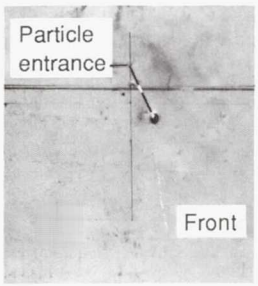

(a) Front of test article.

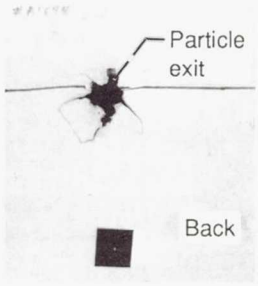

(b) Back of test article.

Figure 6.—Example of damage to coated test article.

HVI Analysis. A penetration correlation for the flow tubes was developed from the phase 2 HVI data on the extrusions. This correlation is based on a modification of the multishock equation given in Ref. 2,

$$d_c = \{1/C\ [6/(\pi\ \rho_p)]\ [\sigma_{y2}/40]^{1/2}\ t_2/V_n(\Sigma S_i)^2\}^{1/3} \qquad (1)$$

The use of this equation is based on the assumption that the damage sustained by the extrusion is primarily due to an impulsive load from the projectile debris, and not primarily from fragment damage. One of the main reasons for using this equation is the multishock configuration of an oblique impact directed through the honeycomb. Because the geometry of the radiator panels is different than the multishock shield configurations which were used to derive the coefficient, C, of Eq. (1), this aspect of the equation was modified based on the test results. The modified Cour-Palais multishock equation to be used as the predictor equation for critical particle size causing radiator tube failure was derived as:

$$d_c = 0.8\ \{[6/(\pi\ \rho_p)]\ [\sigma_{y2}/40]^{1/2}\ t_2/V_n\ S^2\}^{1/3} \qquad (2)$$

or,

$$d_c = C_p \rho_p^{-1/3} V^{-1/3} S^{2/3} t_2^{1/3}\ [\sigma_{y2}/40]^{1/6} \qquad (3)$$

where C_p is 0.993 $(g\text{-}km/(cm^3\text{-}s))^{1/3}$

This equation predicts the particle size causing perforation of the extrusion wall. Particles that do not fail the extrusion can still cause "bulging" or "pinching" of the tube wall or other damage to the interior of the extrusion, although the radiator can continue to operate under these conditions. To prevent any damage to the extrusion interior, the coefficient in Eq. (3) should be decreased by $C_p = 0.68\ (g\text{-}km/cm^3\text{-}s)^{1/3}$.

Evidence to support use of a modified multishock equation includes the primarily impulsive load damage observed on the witness plates mounted behind the panels, and the impulsive load type damage (bulging) observed in the extrusions. The nonperforating damage to the extrusions was manifested in a deformation or bulge that extended into the flow element. No obvious cratering or dimpling from fragment damage was noticeable from the optical examinations of the extrusions.

For small obliquity angles, from 0° to approximately 15°, the projectile will penetrate through a single bumper. Thus, a Cour-Palais Whipple shield predictor (4) was used for determining the critical particle size causing tube failure:

$$d_c = C_n \rho_p^{-1/2} \rho_1^{-1/6} V^{-1} S^{1/2} t_2 [\sigma_{y2}/40]^{1/2}\ , \qquad (4)$$

where the coefficient C_n was modified from experimental results and was found to be 34 $km\text{-}g^{2/3}/(s\text{-}cm^{5/2})$ to prevent tube failure. Tables III and IV contain the results from applying Eqs. (2) and (4) to predict the critical particle size for each of the phase 2 HVI data shots. Equation (2) parameters, such as spacing and obliquity angle, as well as miss distance, are defined in Fig. 7. The difference between actual projectile diameter and calculated critical diameter ($d_p - d_c$) to fail the radiator extrusion and flow tube is also given. When this difference is positive, perforation of the extrusion is predicted. If negative, perforation is not expected, but damage in the form of bulging or pinching without perforation can occur.

TABLE III. - CRITICAL PARTICLE DIAMETER FOR BUMPER DAMAGE

HIRL Shot Number	Projectile Density (g/cc)	Backwall Yield Strength (ksi)	Backwall Thickness (mm)	Vnorm (km/s)	Spacing (mm)	Critical Diameter (dc) (mm)	Projectile Diameter (dp) (mm)	dp - dc (mm)	Bumper Interior Damage *
A1033	2.8	36	0.81	5.5	12.3	1.95	1.42	-0.53	None
A1034				4.2	5.2	1.20	1.59	0.39	Bulge (100%)
A1048				4.6	8.7	1.64	1.00	-0.64	None
A1049				4.5	18.6	2.74	1.59	-1.15	None
A1050				4.4	0.0	Not Calculated	2.38	N/A	Perforated
A1051			↓	4.8	0.0	Not Calculated	1.59	N/A	Perforated
A1052			1.27	4.3	11.6	2.36	2.38	0.02	Perforated
A1054			0.81	4.6	13.7	2.21	1.59	-0.62	Bulge (30%)
A1056			1.27	4.8	5.7	1.41	1.59	0.18	Bulge (10%)
A1057				3.2	8.3	2.09	1.59	-0.50	Slight Bulge (<10%)
A1070			↓	3.5	8.3	2.03	2.38	0.35	Perforated
A1071			0.81	3.2	24.4	3.68	2.00	-1.68	None
A1072				3.3	0.0	Not Calculated	2.00	N/A	Perforated
A1073				3.0	27.9	4.13	2.00	-2.13	None
A1075			↓	3.3	4.2	1.14	2.00	0.86	Perforated
A1089			1.27	3.3	10.6	2.44	2.00	-0.44	Bulge (90%)
A1092			0.81	6.7	0.0	Not Calculated	1.59	N/A	Perforated
A1093				4.9	0.0	Not Calculated	1.59	N/A	Perforated
A1094				4.8	22.2	3.01	2.00	-1.01	Bulge (10%)
A1095			↓	3.7	9.4	1.87	2.00	0.13	Perforated
A1096			1.27	1.7	37.0	6.96	2.38	-4.58	None
A1097	↓		0.81	1.8	23.5	4.39	2.38	-2.01	None
A1098	1.1			4.6	10.1	2.46	2.38	-0.08	Bulge (30%)
A1099	2.8			6.8	0.0	Not Calculated	1.80	N/A	Perforated
A1101			↓	4.7	0.0	Not Calculated	1.80	N/A	Perforated
A1104			1.27	4.7	5.3	1.35	2.00	0.65	Perforated
A1105			0.81	2.4	23.6	3.95	2.00	-1.95	None
A1106				5.1	24.7	3.19	2.00	-1.19	None
A1108			↓	5.0	19.3	2.72	2.00	-0.72	Bulge (20%)
A1109	↓		1.27	4.8	8.1	1.80	2.00	0.20	Perforated
A1185	1.1		0.81	4.0	12.6	2.97	2.38	-0.59	None
A1186	2.8			4.3	1.5	Not Calculated	2.00	N/A	Perforated
A1188	2.8	↓	↓	2.6	13.2	2.62	2.00	-0.62	Bulge (30%)

*Bumper Interior Damage Note : Bulge (x%) = x% closed (estimated)

TABLE IV. - CALCULATED VERSUS ACTUAL PARTICLE DIAMETER FOR FLOW TUBE DAMAGE

HIRL Shot Number	Projectile Density (g/cc)	Backwall Yield Strength (ksi)	Backwall Thickness (mm)	Vnorm (km/s)	Spacing (mm)	Critical Diameter (dc) (mm)	Projectile Diameter (dp) (mm)	dp - dc (mm)	Miss Distance (mm)	Flow Tube Damage *
A1092	2.8	36	0.81	6.7	5.5	1.07	1.59	0.52	0.00	Perforated
A1093	2.8	36	0.81	4.9	5.5	1.19	1.59	0.40	0.00	None
A1094	2.8	36	0.94	4.8	22.2	3.17	2.00	-1.17	9.02	None
A1095	2.8	36	0.94	3.7	9.4	1.96	2.00	0.04	0.03	None
A1099	2.8	36	0.81	6.8	5.5	1.07	1.80	0.73	0.00	Perforated
A1101	2.8	36	0.81	4.7	5.5	1.21	1.80	0.59	0.00	Pinched (100%)
A1185	1.1	36	0.94	4.0	12.6	3.12	2.38	-0.74	2.23	None
A1186	2.8	36	0.81	4.3	5.5	1.24	2.00	0.76	4.62	None
A1188	2.8	36	0.94	2.6	13.2	2.75	2.00	-0.75	2.66	None

*Flow Tube Damage Note : Pinched (x%) = x% closed (estimated)

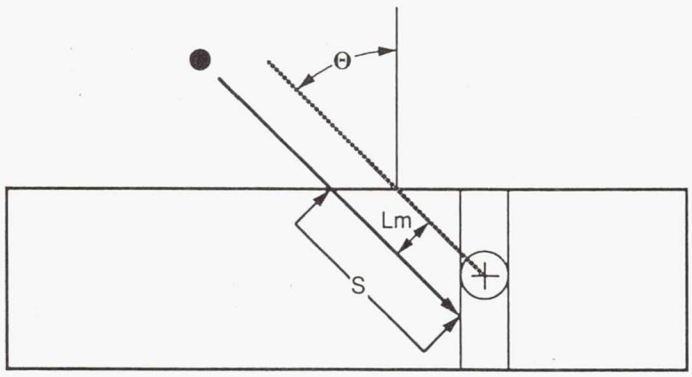

S = spacing: length from front facesheet to the extrusion along the line of flight.
Lm = miss distance between actual line of flight and line of flight to center of extrusion/flow tube.
Θ = obliquity angle of impact.

Figure 7.—Definition of parameters for equation 2.

METEOROID AND DEBRIS HAZARD ANALYSIS

The semi-empirical equations based on the experimental results were used to perform an assessment of the probability of failure of the radiator panel flow tubes from meteoroids and orbital debris. Equations (2) and (4) were used to predict the critical particle size causing complete penetration of the flow tube as a function of obliquity angle for both a thin wall (0.032 in. or 0.8 mm) and thick wall (0.05 in. or 1.3 mm) extrusion. The results are plotted for the thin wall extrusion in Fig. 8 for both meteoroid and debris particles impacting at average velocities of 20 and 10 km/sec, respectively. A similar plot of the thick wall results showed only slightly increased resistance to penetration.

Current Debris Environment

An estimate of the number of impacts from orbital debris and meteoroids on the radiator panel tubes that are large enough to cause failure of the baseline 0.032 in. flow tube extrusion over 10 year period is given in Table V. These data are based on a total flow tube area of 24.78 m^2. The numbers were calculated using the currently baseline space station orbital debris (6) and meteoroid (11) environments. Impact rates from critical particle sizes at both a 400 km (215 nm) operational altitude and the 500 km (270 nm) maximum altitude specified in space station design requirements, (11) are indicated. Table V shows that at the 500 km maximum altitude, the probability of no-failure of

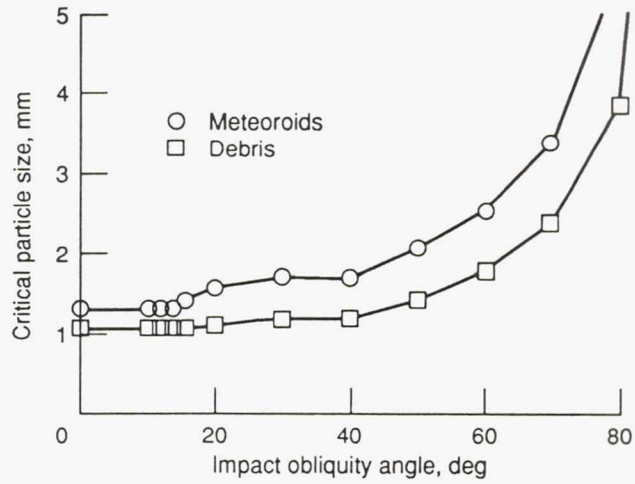

Figure 8.—Particle size causing radiator tube failure.

TABLE V. - METEOROID AND DEBRIS IMPACTS CAUSING FAILURE OF THE SOLAR DYNAMIC RADIATOR PANEL TUBES WITH THIN WALL EXTRUSION
[Thin Wall (0.032 in.) Extrusion, Life: 10 years.]

Radiator case	Surface Area, m^2	Alt., km	Critical particle flux, impacts/m^2-yr		Number of critical impacts over life			Probability of no-failure
			Debris	Met.	Debris	Met	Combined	
Single-loop	12.39	500	5.13×10^{-4}	2.37×10^{-4}	0.064	0.029	0.093	0.911
Either loop (without redundancy)	24.78	500	5.13×10^{-4}	2.37×10^{-4}	.127	.059	.186	.831
Both loops (with redundancy)	24.78	500	-------	-------	-----	-----	.008	.992
Single-loop	12.39	400	1.82×10^{-4}	2.31×10^{-4}	.022	.029	.051	.950
Either loop (without redundancy)	24.78	400	1.82×10^{-4}	2.31×10^{-4}	.045	.057	.102	.903
Both loops (with redundancy)	24.78	400	-------	-------	-----	-----	.002	.9975

TABLE VI. - METEOROID AND DEBRIS IMPACTS CAUSING FAILURE OF THE SOLAR DYNAMIC RADIATOR PANEL TUBES WITH THICK WALL EXTRUSION
[Thick Wall (0.05 in.) Extrusion, Life: 10 years.]

Radiator case	Surface Area, m^2	Alt., km	Critical particle flux, impacts/m^2-yr		Number of critical impacts over life			Probability of no-failure
			Debris	Met.	Debris	Met	Combined	
Single-loop	12.39	500	4.72×10^{-4}	2.21×10^{-4}	0.058	0.027	0.086	0.918
Either loop (without redundancy)	24.78	500	4.72×10^{-4}	2.21×10^{-4}	.117	.055	.172	.842
Both loops (with redundancy)	24.78	500	-------	-------	-----	-----	.007	.993
Single-loop	12.39	400	1.67×10^{-4}	2.15×10^{-4}	.021	.029	.047	.954
Either loop (without redundancy)	24.78	400	1.67×10^{-4}	2.15×10^{-4}	.041	.053	.095	.910
Both loops (with redundancy)	24.78	400	-------	-------	-----	-----	.002	.9979

either of the two loops from orbital debris and meteoroids is 0.83 over 10 years (i.e., there is one chance in six that one of the two loops in each SDR system will fail in 10 years). This was calculated from the individual probability of no-failure of the primary and secondary loops which are both 0.91 over 10 years (i.e., $0.91^2 = 0.83$). The chance that both primary and secondary loops in a SDR system will fail from meteoroids and debris over 10 years is less than 0.8 percent (i.e., 1 - 0.9921). Thus the current design meets the current SDR design requirements.

Similar calculations can be made for the thick walled (0.05") extrusion as given in Table 6. In this case, the probability of failure of an individual loop increases to 0.92 over 10 years at 500 km, which results in an increase to 0.84 of the probability of either loop failing and 0.933 of both loops failing.

More detailed results showing the probability contribution as a function of obliquity angle will be published later this year by the authors.

Sensitivity to Debris Environment. An updated orbital debris environment has been developed from the latest ground-based measurements and returned spacecraft materials.(7) This updated environment is more severe in terms of potential damage than the debris environment (6) currently used for space station design. Adoption of the new debris environment definition is pending final space station approval. Recent activities on the part of the international community in reducing the incidence of catastrophic satellite breakups has resulted in a reduction in the predicted growth of the small debris particle population.(8) Currently, a 2 percent per year growth in the small debris particle population is projected (Kessler, personal communication) versus the 10 percent promulgated in the Kessler, 1989 debris environment definition.

SDR survivability can be significantly affected by the expected growth in the debris environment. The single loop probability of no-failure for the thin wall extrusion (0.032") drops to 0.83 over the 10 years from 2001 to 2010, and to 0.80 from 2011 to 2020. The probability of no failure of either loop drops to 0.69 over 2001 to 2010 and to 0.64 over 2011 to 2020. Probability of failure of both loops becomes 0.97 over 2001 to 2010 and 0.96 over 2011 to 2020.

Discussion of Analysis Assumptions. Several assumptions were made in the penetration assessment analysis that make the calculations conservative (worst case). These include:

(1) Worst case orientation of the oblique impacts was assumed; i.e., perpendicular to the longitudinal axis of the flow tube.

(2) No account was made for added resistance to penetration of the small diameter flow tube relative to the same thickness flat plate.

(3) No account was made for shadowing from the debris and meteoroid flux by the solar dynamic concentrator and other nearby equipment during part of the orbital period.

(4) Recent thermal design optimization of the SDR has reduced the number of panels and number of tubes per panel. Thus the vulnerable area used in these calculations is larger (by at least 15 percent) than that currently expected on-orbit.

Other assumptions tend to increase the uncertainty of the analysis. These include:

(1) The exposed area is equal to the total outside surface area of the flow tubes. This assumption implies that any particle whose original flight line does not intersect with the flow tube will not fail the tube. However, because of the expansion of the debris cloud behind the face sheet, there is a finite probability that a large enough impact occurring on the radiator panel surface can fail a flow tube even if it would not have originally intersected with it. On the other hand, shielding of the SDR by other space station components was also not accounted for.

(2) The actual debris impact angle and velocity distributions encountered by the SDR during on-orbit operations was not accounted for. Average debris velocity and random impact angle assumptions were made in the penetration assessment given in this paper.

(3) The impact response of the flow tubes under HVI testing conditions (i.e., near vacuum - 150 μm pressure, and ambient temperature) versus that of actual on-orbit operating conditions has not been assessed.

CONCLUDING REMARKS

A series of 33 hypervelocity impact tests have been performed in a second phase of testing on representative solar dynamic radiator panel elements to complement test results from more limited first phase testing.

Using current Space Station environment models, (6,11) the panel tubes in the baseline solar dynamic radiator system have a 0.992 reliability (with redundancy) from failure by meteoroid and debris impacts over 10 years. For a single loop, the calculated radiator probability of no-penetration due to hypervelocity impact is 0.83 over 10 years (i.e., 17 percent chance of penetration).

For the updated debris environment (7) with a 2 percent small debris growth rate, the baseline solar dynamic radiator panels have 0.97 probability of no-penetration with redundancy from meteoroid and debris impact over the 10 year period 2001 to 2010. For a single loop, the probability of penetration due to hypervelocity impact is 31 percent.

Increasing the extrusion wall thickness from 0.032 to 0.050 in. provided a very limited increase in protection. Lower velocity tests did not show increased damage when compared to equivalent tests at higher velocities.

The radiator system is made up of more than just the panel tubes. The reliability of the radiator panel interconnect lines and other subsystems exposed to the meteoroid and debris environment should be assessed in a similar hypervelocity impact test and/or analysis procedure, and the results included in an overall assessment of the radiator system reliability.

The second phase of tests has demonstrated that less damage (greater survivability) is observed under HVI test than predicted by available analytical models for the configuration under study. Thus, even limited testing is of value for development of some space hardware.

The HVI test methodology developed for the SDR has been applied to other space station hardware, such as the photovoltaic radiators. Data recorded on damage to aluminum honeycomb is currently being assessed for application to other space station hardware.

ACKNOWLEDGEMENTS

The authors wish to express their gratitude to Jeanne Lee Crews, Manager of the NASA Johnson Space Center Hypervelocity Impact Research Laboratory (HIRL), Burton G. Cour-Palais (MDSSC), and Jim Urbanowicz (LTV) for their contributions to this work.

The authors appreciate the excellent efforts on the part of the HIRL personnel supporting this study including Ken Oser, Earl Brownfield, Joe Falcon, Jay Laughman, Lori Bourassa and Purna Murthy.

REFERENCES

1. Christiansen, E.L. (1990) "Advanced Meteoroid and Debris Shielding Concepts," AIAA Paper 90-1336.

2. Cour-Palais, B.G. and Crews, J.L. (1990). "A Multi-Shock Concept for Spacecraft Shielding," International Journal of Impact Engineering, Vol. 10, pp. 135-146.

3. Cour-Palais, B.G. (1987) "Hypervelocity Impact in Metals, Glass, and Composites," International Journal of Impact Engineering, Vol. 5, pp. 221-237.

4. Cour-Palais, B.G. (1979). "Space Vehicle Meteoroid Shielding Design," Comet Halley Micrometeoroid Workshop, ESA SP-153, European Space Agency, Paris, N. Longdon, ed., pp. 85-92.

5. Crews, J.L. (1990). "HIRL, Hypervelocity Impact Research Laboratory," Information package on the JSC Hypervelocity Impact Research Laboratory (HIRL).

6. Kessler, D.J. (1984) "Orbital Debris Environment for Space Station," NASA Johnson Space Center, JSC-20001, 1984.

7. Kessler, D.J., Reynolds, R.C., and Anz-Meador, P.D. (1988) "Orbital Debris Environment for Spacecraft Designed to Operate in Low Earth Orbit," NASA TM-100471.

8. Kessler, D.J. (1990). "New Orbital Debris Environment," JSC Internal Memorandum, SN3-90-68, May 1.

9. LTV (1989). "Micrometeoroid/Space Debris Impact Analysis for the Solar Dynamic Radiator System," LTV Missiles and Electronics, Report No. 3-46200/9DIR-003.

10. McLallin, K.L., et al. (1988), "The Solar Dynamic Radiator With a Historical Perspective," Proceedings of the 23rd Intersociety Energy Conversion Engineering Conference, Vol. 3, ASME, pp. 335-340. (Also, NASA TM-100972.)

11. NASA (1987) "Space Station Program Natural Environment Definition for Design," NASA Space Station Program Office, Johnson Space Center, JSC-30425, Jan. 15.

12. Parker, V.C. and Crews, J.L. (1987) "Hypervelocity Impact Studies Using a Rotating Mirror Framing Laser Shadowgraph Camera," High Speed Photography, Videography, and Photonics V, H.C. Johnson, ed., SPIE Proc. Vol. 832, Bellingham, WA., pp. 88-95.

13. Rhatigan, J.L., Christiansen, E.L., and Fleming, M.L. (1990). "On Protection of Freedom's Solar Dynamic Radiator from the Orbital Debris Environment, Part 1: Preliminary Analyses and Testing," NASA TM-102458, (also, Proceedings of the 12th Annual International Solar Energy Conference, 1990, pp. 349-356).

14. Secunde, R., Labus, T.L., and Lovely, R.G., (1989) "Solar Dynamic Power Module Design," Proceedings of the 24th Intersociety Energy Conversion Engineering Conference, Vol. 1, IEEE, pp. 299-307. (Also, NASA TM-102055.)

NASA
National Aeronautics and Space Administration

Report Documentation Page

1. Report No.	2. Government Accession No.	3. Recipient's Catalog No.
NASA TM-104514		

4. Title and Subtitle
On Protection of Freedom's Solar Dynamic Radiator from the Orbital Debris Environment
Part 2: Further Testing and Analyses

5. Report Date

6. Performing Organization Code

7. Author(s)
Jennifer L. Rhatigan, Eric L. Christiansen, and Michael L. Fleming

8. Performing Organization Report No.
E-6335

10. Work Unit No.
474-52-10

9. Performing Organization Name and Address
National Aeronautics and Space Administration
Lewis Research Center
Cleveland, Ohio 44135-3191

11. Contract or Grant No.

13. Type of Report and Period Covered
Technical Memorandum

12. Sponsoring Agency Name and Address
National Aeronautics and Space Administration
Washington, D.C. 20546-0001

14. Sponsoring Agency Code

15. Supplementary Notes
Prepared for the International Solar Energy Conference sponsored by the American Society of Mechanical Engineers, Lahaina, Maui, Hawaii, April 4-8, 1992. Jennifer L. Rhatigan, NASA Lewis Research Center; Eric L. Christiansen, NASA Lyndon B. Johnson Space Center, Houston, Texas 77058; Michael L. Fleming, LTV Missiles and Electronics, Dallas, Texas 75265. Responsible person, Jennifer L. Rhatigan, (216) 433-8330.

16. Abstract
Recent progress to better understand the environmental threat of micrometeoroid and space debris to the radiator for the solar dynamic power system on Space Station Freedom is reported. The objective has been to define a design which would perform to survivability requirements over the expected lifetime of the radiator. A previous paper described the approach developed to assess on-orbit survivability of the solar dynamic radiator due to micrometeoroid and space debris impacts. Preliminary analyses were presented to quantify the solar dynamic radiator survivability. These included the type of particle and particle population expected to defeat the radiator bumpering. Results of preliminary hypervelocity impact (HVI) testing performed on radiator panel samples were also presented. This paper presents results of a more extensive test program undertaken to further define the response of the solar dynamic radiator to HVI. Tests were conducted on representative radiator panels (under ambient, nonoperating conditions) over a range of velocity. Target parameters were also varied. Data indicate that analytical penetration predictions are conservative (i.e., pessimistic) for the specific configuration of the solar dynamic radiator. Test results are used to define the solar dynamic radiator reliability with respect to HVI more rigorously. Test data, analyses, and survivability results are presented.

17. Key Words (Suggested by Author(s))	18. Distribution Statement
Space radiators; Hypervelocity impact; Spacecraft survivability; Solar dynamic power systems; Space debris; Micrometeroids; Aerospace environments	Unclassified - Unlimited Subject Category 20

19. Security Classif. (of the report)	20. Security Classif. (of this page)	21. No. of pages	22. Price*
Unclassified	Unclassified	10	A03

NASA FORM 1626 OCT 86

*For sale by the National Technical Information Service, Springfield, Virginia 22161